*Ersch. in: Journal of molecular structure ; 485-486 (1999). - S. 409-419*

*http://dx.doi.org/10.1016/S0022-2860(99)00184-2*

# Alternative force field models for ansa-zirconocene complexes—vibrational and structural studies on $Me_2Si$-bridged and *tert*-butyl-substituted representatives

H.-H. Brintzinger*, M.-H. Prosenc, F. Schaper, A. Weeber, U. Wieser

*Fakultät für Chemie, Universität Konstanz, D-78457 Konstanz, Germany*

Dedicated to Professor Lawrence S. Bartell on the occasion of his 75th birthday

**Abstract**

A force field model for ansa-zirconocene complexes is constructed, which represents each C atom of the $C_5$-ring ligands as being bonded directly to the metal center, rather than by way of the $C_5$-ring centroids. This $\eta^5$-model, which describes coordination geometries by mutual repulsions of the $C_5$-ring and halide ligands, has no adjustable equilibrium or force-constant parameters for any of the angles at the Zr center. Nevertheless, vibrational frequencies and structural parameters are reproduced for a series of simple and $Me_2Si$-bridged zirconocene dihalide complexes with an accuracy comparable to that of the more complex centroid model. Strong steric distortions, revealed by crystal structure determinations in a series of *tert*-butyl-substituted ansa-zirconocene dibromide and diiodide complexes, are likewise reproduced with remarkable accuracy by the $\eta^5$-force field model.

*Keywords:* Zirconocene complexes; Ansa-metallocenes; Molecular-mechanics models; Force field parameters; Molecular vibrations; Crystal structures

## 1. Introduction

Among the many topics investigated by Bartell and coworkers with regard to coordination geometries, one concerns the deviations of group IV metallocene complexes from axial symmetry [1]. Group IV metallocene complexes, especially their ring-bridged "ansa"-derivatives, have recently gained interest as stereoselective catalysts, e.g. for α-olefin polymerizations [2]. In this context, the geometry of the metallocene complex, e.g. the steric accessibility of its coordination sites—appears to be essential for the activity and stereoselectivity of the ensuing catalyst systems.

In order to predict the geometries of variously substituted and ring-bridged zirconocene complexes, several recent studies have described molecular-mechanics models for ansa-metallocene complexes [3–9]. In all of these studies, a force field is utilized where the metal center is connected to each of the $C_5$-ring ligands by a pseudo-bond to the respective $C_5$-ring centroid. This connectivity scheme has been shown to afford rather accurate descriptions of inter-ring angles and of rotational conformations for a variety of cyclopentadienyl complexes [5–17]. Closer to chemical intuition, however, would appear to be a force field in which each cyclopentadienyl C atom is

* Corresponding author. Tel.: + 49-7531-882-629; fax: + 49-7531-883-137.

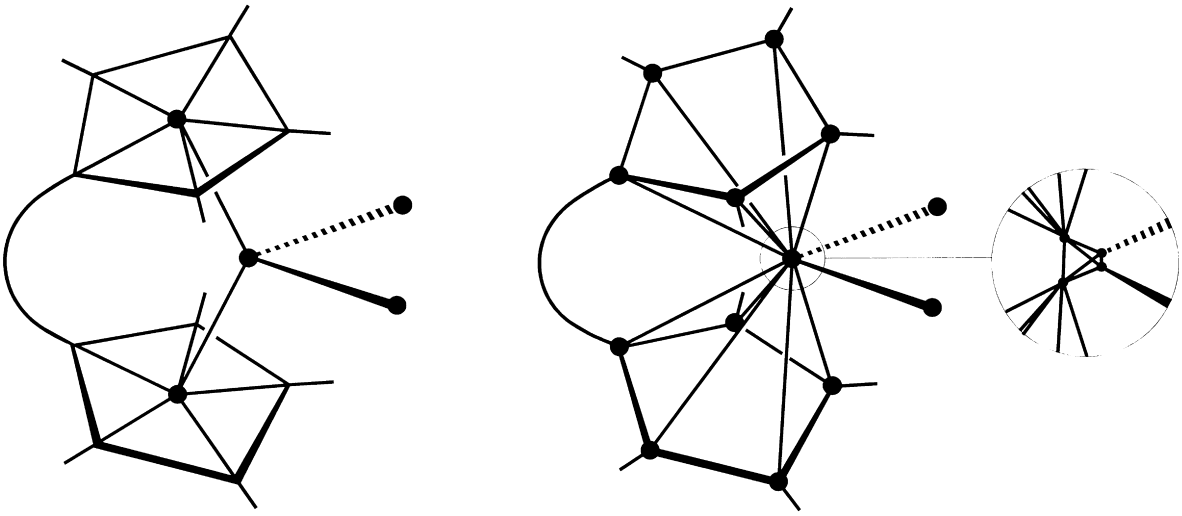

Fig. 1. Schematic representations of the centroid force field model (left) and of the $\eta^5$ force field model (right, with split-up central atom shown in insert).

connected directly to the Zr center, such that distortions—caused for example by steric repulsions—are controlled by the "elasticity" of the individual Zr–C bonds rather than by that of the fictional metal–centroid–carbon "bond" angle.

That an $\eta^5$-connectivity scheme can lead to adequate structural predictions has been shown by Allinger and coworkers for a series of main-group and lanthanoid metallocenes [18]. In this communication we want to describe a $\eta^5$-type force field for ring-bridged zirconocene complexes, to calibrate it with the help of vibrational data, and to compare its structural predictions to those of a centroid-based model.

## 2. Results and discussion

### *2.1. Alternative force field models*

The adoption of an $\eta^5$-force field instead of a centroid model has the corollary that the mutual disposition of the $C_5$-ring ligands cannot be determined by centroid–metal–centroid nor by the—widely varying—inter-ring C–Zr–C angles. Instead, the coordination geometry of such a complex has to be reproduced by mutual repulsions of the $C_5$-ring ligands with each other and with the other ligands present. Van-der-Waals-interactions of this type are commonly used to describe coordination geometries [15–23] and have also been shown to afford satisfactory structural descriptions for complexes with cyclopentadienyl ligands [8–18].

Not all of the commercially available molecular-mechanics programs take account, however, of mutual repulsions between atoms bound to a common center, as these are normally incorporated into the angle bending parameters. While options to include these 1,3-repulsive interactions are provided in some programs designed especially for coordination compounds [18,24–26], a generally applicable way to circumvent this problem is to replace the metal center with a small cluster of pseudo-metal atoms fixed at an infinitesimally small distance from each other [23].

In following this strategy, we have used, instead of a central Zr atom, a small tetrahedron of four Zr/4 centers (each with $m = 22.8$ amu), fixed at a mutual distance of 0.01 pm. Two of these centers are each joined to one halogen ligand X while each of the other two carries five bonds to the C atoms of one cyclopentadienyl ring, with identical Zr–C bond length and stretching parameters and with all bending and torsional force constants involving a Zr center being set to zero (Fig. 1).

For the construction and the vibrational and structural analyses of the zirconocene complexes

Table 1
Van-der-Waals parameters used for the Lennard-Jones function $E_{vdW} = (A_{ij}/r_{ij}^{12}) - (B_{ij}/r_{ij}^{6})$

| Van-der-Waals | $A_{ij}$ (kcal mol$^{-1}$ Å$^{12}$) | $B_{ij}$ (kcal mol$^{-1}$ Å$^{6}$) |
|---|---|---|
| F | 800000.0 | 235.2 |
| Cl | 9000000.0 | 541.0 |
| Br | 20000000.0 | 1195.0 |
| I | 70000000.0 | 2400.0 |
| CC | 18000000.0 | 1124.0 |

considered, we have used the BIOSYM program package [27], which provides the algorithms required for vibrational analyses and allows, in its geometry optimization parts, to accommodate even substantial deviations from the Zr–C and Zr–centroid equilibrium distances by use of a Morse potential. For most of the internal bonds of the organic ligands, standard parameters provided in the BIOSYM program package were used; exceptions are listed in Tables 1–4. In lieu of the missing angular parameters, the van-der-Waals radii of the halide ligands (i.e. the Lennard-Jones parameters *A* listed in Table 1) were used as adjustable entities and chosen so as to give acceptable X–Zr–X angles for the $\eta^5$-model. Partial charges, adapted from semi-empirical Zindo-1 calculations, of −0.04, +0.80 and −0.20 units were placed on C, Zr and halogen atoms, respectively, to facilitate assignments of the vibrational modes by comparison of calculated and observed intensities. Vibrational frequency calculations were not significantly affected by these charges. The non-standard parameters derived for the alternative force fields from the following vibrational and structural analyses are presented in Tables 1–4. It should be noted that all calculations were done on isolated complexes, thus representing more the behavior in the gas phase than in the solid state.

Table 3
Bond angle and bending force constants used for the quadratic function $E_{ang} = k(\vartheta - \vartheta_0)^2$

| | $\vartheta_0$ (°) | $k$ (kcal mol$^{-1}$ rad$^{-2}$) |
|---|---|---|
| CC–CC–CC | 108.0 | 31.0 |
| Si–CC–CC | 126.0 | 21.0 |
| C–CC–CC | 126.0 | 26.0 |
| C–C–CC | 109.5 | 32.5 |
| CC–Si–CC | 109.5 | 70.0 |
| C–Si–CC | 109.5 | 21.5 |
| F–Zr–F[a] | 105.0 | 40.0 |
| Cl–Zr–Cl[a] | 105.0 | 50.0 |
| Br–Zr–Br[a] | 105.0 | 60.0 |
| I–Zr–I[a] | 105.0 | 60.0 |
| F–Zr–CR[a] | 100.0 | 15.0 |
| Cl–Zr–CR[a] | 100.0 | 30.0 |
| Br–Zr–CR[a] | 100.0 | 30.0 |
| I–Zr–CR[a] | 100.0 | 40.0 |
| CR–Zr–CR[a] | 128.0 | 15.0 |
| CC–CR–ZR[a] | 90.0 | 35.0 |

[a] For the centroid model only.

Table 2
Bond length and stretching force constants used for the Morse function $E_{str} = D[1 - \exp(-\alpha(r - r_0))]^2$

| | Centroid model | | | $\eta^5$ model | | |
|---|---|---|---|---|---|---|
| | $r_0$ (Å) | $D$ (kcal mol$^{-1}$) | $\alpha$ (Å$^{-1}$) | $r_0$ (Å) | $D$ (kcal mol$^{-1}$) | $\alpha$ (Å$^{-1}$) |
| Zr–F[a] | 1.92 | 70 | 1.79 | 1.93 | 70 | 1.90 |
| Zr–Cl[a] | 2.33 | 70 | 1.32 | 2.29 | 70 | 1.44 |
| Zr–Br[a] | 2.51 | 70 | 1.34 | 2.47 | 70 | 1.38 |
| Zr–I[a] | 2.65 | 70 | 1.06 | 2.63 | 70 | 1.27 |
| Zr–CR | 2.13 | 100 | 2.03 | | | |
| CR–CC | 1.21 | 70 | 2.00 | | | |
| Zr–CC | | | | 2.38 | 20 | 1.85 |
| Zr–Zr | | | | 0.0001 | 100 | 20.00 |
| CC–C | 1.50 | 70 | 2.13 | 1.50 | 70 | 2.13 |
| CC–H | 1.10 | 70 | 2.13 | 1.10 | 70 | 2.13 |
| Si–C | 1.85 | 70 | 2.00 | 1.85 | 70 | 2.00 |
| Si–CC | 1.87 | 70 | 1.90 | 1.87 | 70 | 1.90 |

[a] Minor differences of the Zr–X bond length parameters for the two models are due to the lack of 1–3 repulsion between halogen atoms in the centroid model.

Table 4
Torsion angles, force constants and multiplicities used for the function $E_{tor} = V[1 + \cos(n\Phi - \Phi_0)]$

| | $k$ (kcal mol$^{-1}$) | $\Phi_0$ (°) | $n$ |
|---|---|---|---|
| H–CC–CC–CC | 7.50 | 180.0 | 2 |
| C–CC–CC–CC | 8.00 | 180.0 | 2 |
| Si–CC–CC–CC | 5.00 | 180.0 | 2 |
| CC–CC–CC–CC | 8.00 | 180.0 | 2 |
| CC–CR–CC–CC | 10.00 | 180.0 | 2 |
| H–CC–CC–H | 2.00 | 0.0 | 2 |

### *2.2. Vibrational analysis*

To calibrate the force constant parameters for both force fields, infra-red spectra for the previously studied unbridged complexes $(C_5H_5)_2ZrX_2$ (**1A**–**D**, with X = F, Cl, Br, I) [28–33] were remeasured for comparison with those of their dimethylsilyl-bridged zirconocene counterparts $Me_2Si(C_5H_4)_2ZrX_2$ (**1B**–**D**). Comparison of the spectra obtained for these seven complexes (Fig. 2), especially the almost constant frequencies of Zr–Cp stretching, ring-tilt and deformation modes and the systematic frequency variation of the Zr–X stretching, scissoring and wagging vibrations lead, in accord with earlier studies on the unbridged species $(C_5H_5)_2ZrX_2$ [28–33], to the assignments listed in Table 5. These assignments are further supported by calculations of the frequencies of all vibrational modes in complexes **1B** and **2B** by density-functional methods [34]. Characteristic of the $Me_2Si$-bridged complexes **2B**–**D** are two strong bands at ca. 450 and 420 cm$^{-1}$, which we assign to symmetric and asymmetric ring-tilt modes coupled to Si-ring stretching vibrations.

As shown in Table 5, the frequencies of the characteristic vibrations for all seven complexes are reproduced with reasonable accuracy by both force field models with the appropriate choice of parameters (cf. Tables 1–4). For the depth of the Morse potential, an estimated average value of $D = 70$ kcal/mol was used for all Zr–halogen bonds [35]. For the Zr–centroid bond, $D = 100$ kcal/mol was chosen, corresponding to available estimates for metal–Cp dissociation energies [36], while one-fifth of this value was used for each Zr–C bond in the $\eta^5$-model. The respective stretching frequencies, which depend on the parameters $D$ and $\alpha$ according to the expression $D\alpha^2$, were then used to determine optimal values of $\alpha$.

For the centroid model, bending force constants for the X–Zr–X, centroid–Zr–centroid and Zr–centroid–carbon angles were calibrated by minimizing the differences between observed and calculated frequencies for the X–Zr–X and Cp–Zr–Cp deformations and for the ring tilting modes, respectively.

In the $\eta^5$-model, which does not contain any adjustable angular force constants of this type, the X–Zr–X and Cp–Zr–Cp deformation frequencies depend only on the inter-ligand repulsion forces. Remarkably enough, we obtain rather satisfactory values for the frequencies for these deformation modes with the van-der-Waals parameters chosen so as to give X–Zr–X equilibrium angles in the correct range. Similarly, rather reasonable frequencies are calculated for the ring tilting modes by use of the Zr–C stretching force constant derived from the Zr–Cp stretching frequencies. Further improvement of these results could presumably be achieved (but was not attempted) by additional adjustments of the van-der-Waals parameters also of the ring-C atoms or by use of a more elaborate van-der-Waals potential function, e.g. of the Buckingham type.

The remarkable fit obtained indicates to us that mutual ligand repulsion is indeed an adequate descriptor not only for the equilibrium geometry but also for the deformability of metallocene complexes, at least of the formally $d^0$-configurated species considered here. That a single Zr–C stretching force constant describes both types of Zr-ring deformation modes with comparable accuracy as the combined Zr–centroid stretching and Zr–centroid–carbon bending force constants invoked in the centroid model can likewise be taken as an indication that

Fig. 2. Infrared spectra of the unbridged zirconocene halide complexes **1A**–**1D** (top) and of their $Me_2Si$-bridged analogs **2B**–**2D** (bottom). Dotted lines point to the Zr–Cp stretching, deformation and ring-tilt vibrations, shaded areas represent Zr–halogen stretching vibrations.

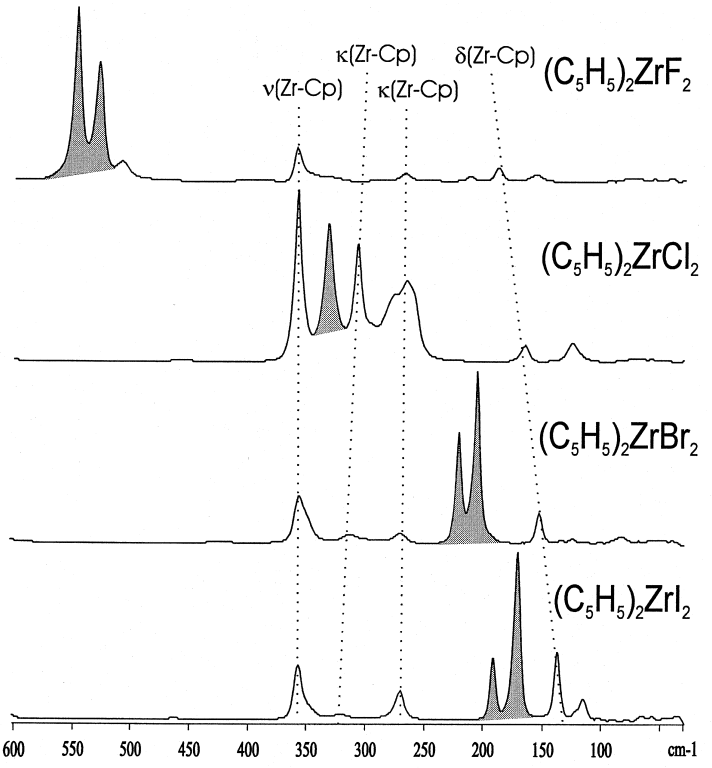
ν(Zr-Cp)
κ(Zr-Cp)
κ(Zr-Cp)
δ(Zr-Cp)
(C5H5)2ZrF2
(C5H5)2ZrCl2
(C5H5)2ZrBr2
(C5H5)2ZrI2
600 550 500 450 400 350 300 250 200 150 100 cm-1

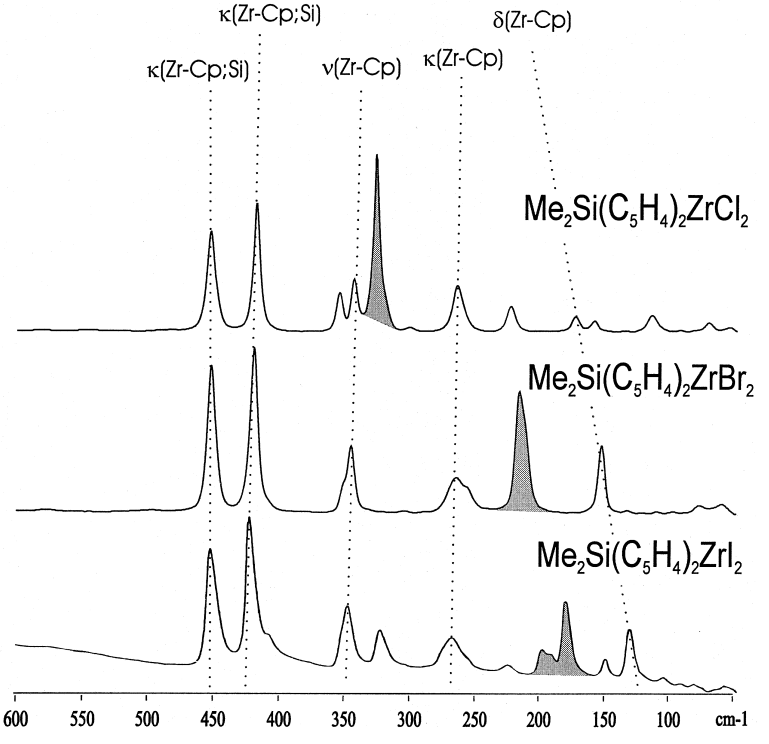
κ(Zr-Cp;Si)
κ(Zr-Cp;Si)
ν(Zr-Cp)
κ(Zr-Cp)
δ(Zr-Cp)
Me2Si(C5H4)2ZrCl2
Me2Si(C5H4)2ZrBr2
Me2Si(C5H4)2ZrI2
600 550 500 450 400 350 300 250 200 150 100 cm-1

the actual bonding situation in these complexes is more closely approached by the $\eta^5$-model.

### 2.3. Structural analysis

Structural data available for complexes **1A**–**D** and **2B** [37–40] were used to calibrate the equilibrium bond length and angle parameters listed in Tables 1–4. As shown in Table 6, both force fields reproduce the coordination geometries of these five unsubstituted zirconocene complexes with comparable accuracy.

As a test for the ability of the alternative force fields to predict structural distortions of ansa-zirconocene

Table 5
Vibrational frequencies observed for unbridged zirconocene halides **1A**–**1D** and for their $Me_2Si$-bridged analogs **2B**–**2D** (bold figures; s = strong, m = medium, w = weak) and frequencies calculated with the centroid model (straight figures) and with the $\eta^5$-model (figures in italics); with root-mean-square deviations listed in the last two lines ($\nu$ = stretching modes; $\kappa$ = ring-tilt modes; $\delta$ = deformation modes)

| Mode | **1A** | **1B** | **1C** | **1D** | **2B** | **2C** | **2D** |
|---|---|---|---|---|---|---|---|
| $\nu_{as}$ (Zr–Cp) | **360 (m)** | **358 (s)** | **357 (m)** | **358 (m)** | **344 (m)** | **346 (s)** | **347 (s)** |
| | 360 | 358 | 357 | 358 | 351 | 351 | 349 |
| | *373* | *358* | *360* | *358* | *331* | *333* | *327* |
| $\nu_s$ (Zr–Cp)[a] | **360 (m)** | **358 (s)** | **357 (s)** | **358 (m)** | | | |
| | *361* | *363* | *363* | *362* | | | |
| $\nu_s$ (Zr–X)[b] | **547 (s)** | **332 (s)** | **221 (s)** | **192 (m)** | | | **200 (m)** |
| | 539 | 330 | 230 | 216 | | | 229 |
| | *556* | *330* | *228* | *202* | | | *198* |
| $\nu_{as}$ (Zr–X) | **529 (s)** | **332 (s)** | **205 (s)** | **172 (s)** | **327 (s)** | **217 (s)** | **181 (s)** |
| | 535 | 332 | 200 | 163 | 326 | 192 | 158 |
| | *522* | *332* | *189* | *163* | *326* | *190* | *162* |
| $\kappa$ (Zr–Cp) | **291 (w)** | **307 (s)** | **314 (w)** | **321 (w)** | **301 (w)** | **303 (w)** | **323 (n)** |
| | 299 | 281 | 313 | 304 | 323 | 284 | 274 |
| | *299* | *276* | *313* | *308* | *291* | *298* | *288* |
| ($\kappa$ (Zr–Cp) | **268 (w)** | **266 (s)** | **270 (w)** | **271 (m)** | **265 (m)** | **266 (m)** | **269 (m)** |
| | 262 | 251 | 264 | 256 | 282 | 239 | 266 |
| | *266* | *253* | *264* | *263* | *268* | *275* | *270* |
| $\delta$(Zr–Cp) | **189 (m)** | **165 (m)** | **153 (m)** | **138 (m)** | **175 (w)** | **154 (m)** | **132 (m)** |
| | 181 | 186 | 148 | 111 | 186 | 148 | 111 |
| | *168* | *184* | *164* | *143* | *160* | *137* | *121* |
| $\delta$ (Zr–X)[c] | **212 (w)** | **165 (m)** | **125 (w)** | **116 (m)** | **160 (w)** | **134 (w)** | **107 (w)** |
| | 208 | 158 | 122 | 97 | 147 | 119 | 96 |
| | *229* | *165* | *148* | *129* | *154* | *137* | *125* |
| $\delta$ (Zr–X)[d] | **157 (w)** | **125 (m)** | **83 (w)** | **66 (w)** | **116 (w)** | **79 (w)** | **59 (w)** |
| | 161 | 125 | 84 | 63 | 118 | 80 | 59 |
| | *177* | *144* | *100* | *80* | *119* | *83* | *68* |
| $\kappa_{as}$(Zr–Cp;Si)[e] | | | | | **453 (s)** | **453 (s)** | **452 (s)** |
| | | | | | 403 | 402 | 402 |
| | | | | | *415* | *415* | *414* |
| $\kappa_s$(Zr–Cp;Si)[e] | | | | | **419 (s)** | **420 (s)** | **421 (s)** |
| | | | | | 367 | 361 | 360 |
| | | | | | *403* | *402* | *398* |
| RMS dev. | 6 | 13 | 5 | 16 | 27 | 30 | 33 |
| | *13* | *14* | *12* | *10* | *16* | *19* | *23* |

[a] $\nu_s$ (Zr–Cp) mode is not obtained in the centroid model.
[b] $\nu_s$ (Zr–X) mode is not observed in complexes **2B** and **2C**.
[c] Rocking and/or wagging modes.
[d] Scissoring mode.
[e] Ring-tilt modes coupled with Si–C stretching modes.

Table 6
Bond lengths (in pm) and angles (in degrees), observed in the unbridged zirconocene dihalides **1A**–**1D** and in the $Me_2Si$-bridged dichloride **2A** (bold figures [35–39]) and corresponding values calculated with the centroid model (straight figures) and with the $\eta^5$ model (figures in italics)

| | **1A** | **1B** | **1C** | **1D** | **2A**[a] |
|---|---|---|---|---|---|
| Bond lengths | | | | | |
| Zr–X | **197** | **244** | **261** | **283** | **244** |
| | 197 | 245 | 262 | 284 | 243 |
| | *198* | *244* | *262* | *284* | *241* |
| Zr–C1 | **252** | **252** | **252** | **251** | **255** |
| | 252 | 253 | 252 | 250 | 258 |
| | *250* | *250* | *249* | *253* | *255* |
| Zr–C2 | **250** | **251** | **250** | **251** | **254** |
| | 252 | 252 | 252 | 252 | 258 |
| | *248* | *250* | *249* | *250* | *255* |
| Zr–C3 | **250** | **249** | **249** | **249** | **247** |
| | 250 | 251 | 251 | 251 | 249 |
| | *248* | *250* | *249* | *249* | *247* |
| Zr–C4 | **250** | **248** | **248** | **245** | **247** |
| | 250 | 250 | 250 | 250 | 249 |
| | *248* | *248* | *247* | *247* | *247* |
| Zr–C5 | **250** | **247** | **246** | **243** | **247** |
| | 249 | 249 | 249 | 249 | 243 |
| | *248* | *248* | *247* | *247* | *245* |
| Zr–CR[b] | **220** | **220** | **220** | **219** | **220** |
| | 219 | 220 | 220 | 220 | 220 |
| Bond angles | | | | | |
| X–Zr–X | **96** | **97** | **97** | **96** | **98** |
| | 93 | 94 | 96 | 95 | 97 |
| | *91* | *90* | *90* | *90* | *92* |
| CR–Zr–CR[b] | **131** | **127** | **129** | **126** | **125** |
| | 129 | 128 | 128 | 128 | 127 |

[a] Si–C and Si–CC distances of 185 and 187 pm and C–Si–C and CC–Si–CC angles of 116 and 93°, respectively, are exactly reproduced by both models (CC = cyclopentadienyl C-atom; C = methyl C-atom).
[b] CR = $C_5$-ring centroid.

complexes, we have determined the structures of the *tert*-butyl-substituted ansa-zirconocene bromides and iodides, rac-$Me_2Si(3\text{-}^tBu\text{–}C_5H_3)_2ZrX_2$ (**3C,D**) and rac-$Me_2Si(2\text{-Me-}4\text{-}^tBu\text{–}C_5H_2)_2ZrX_2$ (**4C,D**). These complexes were selected for the present purpose since they combine particularly large Zr-bound ligands with bulky $C_5$-ring substituents.

The results of the respective diffractometric analyses (Fig. 3, Table 7) reveal substantial variations of the Zr–C distances in these complex molecules: In each of the bromide and iodide complexes, the bonds to the *tert*-butyl-substituted ring-C atoms are elongated by ca. 20 pm. The planarity of the $C_5$ rings causes the neighboring Zr–C distances to be likewise increased, although to a lesser extent, while essentially unchanged Zr–C distances of 245–250 pm are found for the C atoms in the bridgehead and in one of the neighboring $\alpha$-positions. Associated with these distortions is a substantial out-of-plane bending of the C–C bond carrying the *tert*-butyl-substituents as well as a tilting of the latter.

Quite remarkable is a deviation of the overall structures of some of the complexes from the expected $C_2$ symmetry in that the bridging Si atom deviates substantially from the $ZrX_2$ bisector plane. This type of distortion has been observed before in ansa-titanocene compounds [15,41] but is conspicuously absent in the related ansa-zirconocene dichloride **4B** [42]. It is particularly pronounced for the dibromide complexes **3C** and **4C** and for the diiodide complex **3D**. In the diiodide **4D**, repulsion of the large iodide ligands by the $\alpha$-positioned methyl groups appears to suppress this distortion altogether.

The mutually balanced steric repulsions and bond length and angle deformations—e.g. the increased Zr–C distances documented by the data in Table 7—are reproduced with satisfactory accuracy by both of the force fields studied (cf. Fig. 4 and Table 7). Most gratifying is, in particular, that the angle of ca. 20°, by which the Si–Zr axis deviates from the $ZrX_2$ bisector plane in the dibromide and diiodide compexes **3C** and **3D**, is equally well reproduced by both models, as is the suppression of this distortion in the $\alpha$-methyl substituted diiodide complex **4D** and its absence in the difluoride and dichloride complexes **4A** and **4B**, for which axially symmetric geometries have been determined (cf. Ref. [42] and Section 3).

Our results document that the $\eta^5$-force field presented above can describe the geometries of simple and sterically distorted ansa-zirconocene complexes in great detail, with an accuracy comparable to that of the previously developed centroid model. Even though we have investigated here only a limited number of complex molecules, the results obtained let it appear worthwhile to establish and parametrize similar $\eta^5$-force field algorithms also in other program packages for use in the molecular modelling of catalyst systems based on ansa-metallocene and related complexes. In this regard we note that conversion of the dichloride complex **1B** to the dimethyl

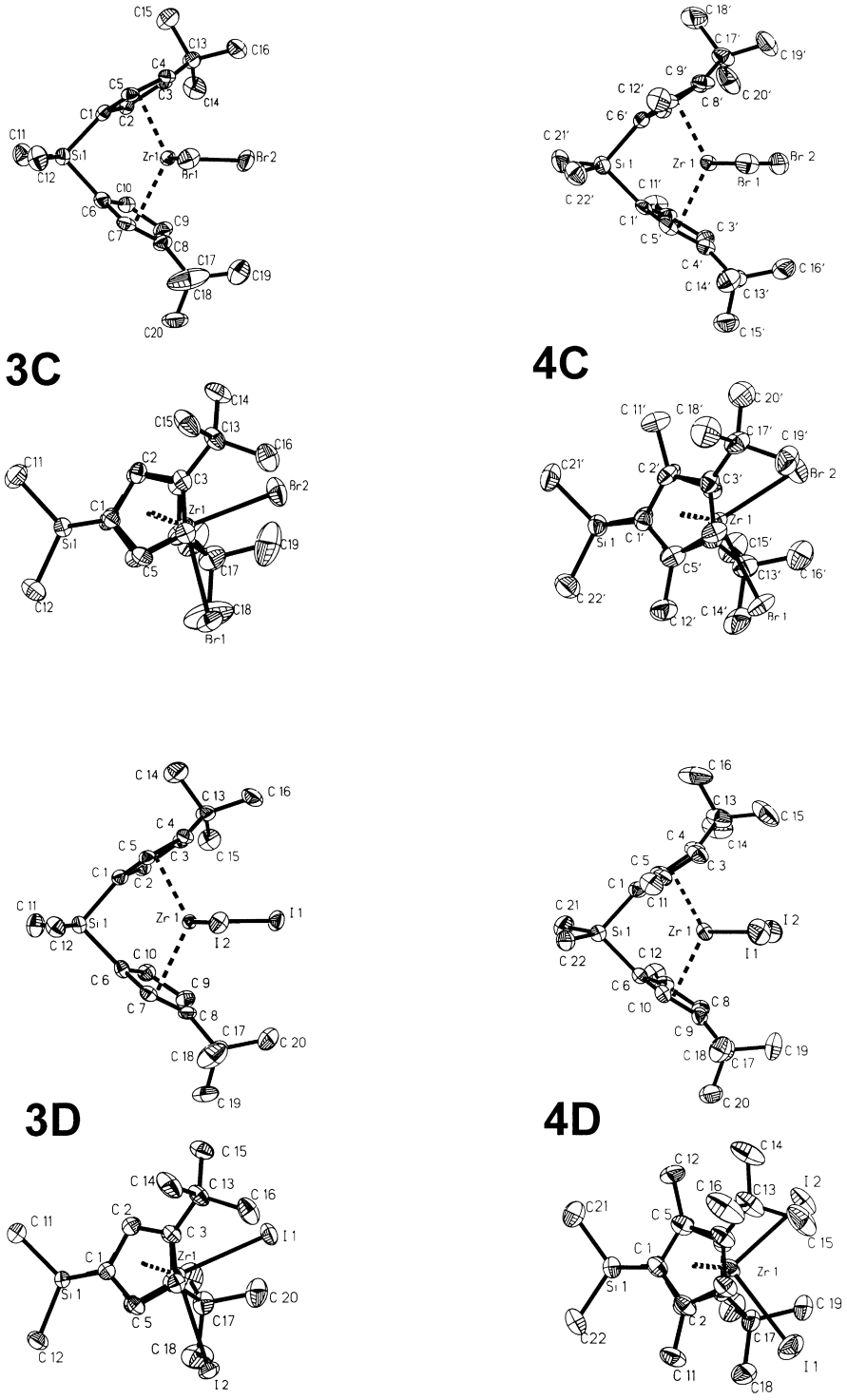


Fig. 3. Crystal structures of the dibromide complexes **3C** and **4C** (top), and of the diiodide complexes **3D** and **4D** (bottom) projected (with H atoms omitted) on the $ZrX_2$ plane and on the centroid–Si–centroid plane.

complex $(C_5H_5)_2Zr(CH_3)_2$ shifts the Zr–Cp stretching vibration only slightly, from 358 to 339 $cm^{-1}$, while formation of a catalytically active contact ion pair, $(C_5H_5)_2Zr(CH_3)^+\cdots H_3C{-}B(C_6F_5)_3^-$ [43,44], by addition of one equivalent of $B(C_6F_5)_3$ restores this vibrational frequency to its previous value of 358 $cm^{-1}$. The Zr–$C_5$ stretching force constants obtained for the series of halide complexes considered here are thus likely to be sufficiently accurate also for other zirconocene species of interest in catalysis.

## 3. Experimental

The difluoride complex **1A** and the dichloride complexes **1B**, **2B**, **3B** and **4B** were synthesized as described before [30,41,42,45–47]. The dichlorides were converted, by reaction with excess $BBr_3$ and $BI_3$ [30], to the corresponding dibromo and diiodo derivatives, respectively, which were obtained, NMR-spectrally pure, in the form of green and orange crystals, respectively.

For the measurement of their infrared spectra, the zirconocene complexes were incorporated into polyethene pellets. IR spectra were recorded, in the "sample shuttle" mode [48] with a resolution of 4 $cm^{-1}$, on a Perkin–Elmer 2000 FT-IR spectrometer.

Crystals of the racemic isomers of complexes **3C**, **3D**, **4C** and **4D**, which were suitable for X-ray structure determinations, were obtained by crystallization from pentane. Experimental conditions and results of the determination of these crystal structures are summarized in Table 8, selected bond distances and angles in Table 7. Two crystallographically independent molecules with almost identical geometries are found in the unit cell of compounds **3C**, **3D** and **4C**. The structures of one molecule of each of these complexes and that of complex **4D** are represented in Fig. 3. Further details of the structures, such as atomic position and isotropic and anisotropic thermal

Table 7
Bond lengths (in pm) and bond angles (in degrees) observed for the dibromides **3C** and **4C** and the diiodides **3D** and **4D** (bold figures) and corresponding values calculated with the centroid model (straight figures) and the $\eta^5$ model (figures in italics) (Si–C and Si–CC distances of 184–186 pm and 186–187 pm and C–Si–C and CC–Si–CC angles of 110–113° and 95–97°, respectively, are reproduced by both models within the experimental error range)

| | **3C** | **3D** | **4C** | **4D** | | **3C** | **3D** | **4C** | **4D** |
|---|---|---|---|---|---|---|---|---|---|
| Bond lengths | | | | | Bond angles | | | | |
| Zr–X | **259** | **282** | **258** | **283** | X–Zr–X | **97** | **96** | **96** | **95** |
| | 259 | 280 | 259 | 279 | | 96 | 95 | 97 | 96 |
| | *259* | *280* | *258* | *279* | | *90* | *92* | *91* | *92* |
| Zr–C1 | **265** | **267** | **264** | **267** | CR–Zr–CR[a] | **125** | **126** | **126** | **126** |
| | 265 | 267 | 265 | 268 | | 127 | 127 | 129 | 129 |
| | *265* | *268* | *266* | *269* | | | | | |
| Zr–C2 | **257** | **258** | **259** | **260** | C(*t*Bu)–CC–Pl(1)[a] | **18** | **16** | **16** | **15** |
| | 260 | 261 | 262 | 263 | | 19 | 19 | 15 | 15 |
| | *258* | *261* | *262* | *265* | | *18* | *17* | *16* | *14* |
| Zr–C3 | **250** | **253** | **252** | **251** | Si–CC–Pl(1)[a] | **11** | | | |
| **14** | **10** | **14** | | | | | | | |
| | 253 | 254 | 251 | 252 | | 12 | 14 | 14 | 15 |
| | *251* | *254* | *250* | *252* | | *12* | *13* | *12* | *14* |
| Zr–C4 | **244** | **243** | **247** | **250** | | | | | |
| | 244 | 243 | 245 | 245 | | | | | |
| | *244* | *244* | *246* | *247* | | | | | |
| Zr–C5 | **244** | 243 | **246** | **247** | | | | | |
| | 239 | 239 | 238 | 238 | | | | | |
| | *242* | *242* | *241* | *242* | | | | | |
| Zr–CR[a] | **222** | **223** | **223** | **224** | | | | | |
| | 221 | 222 | 222 | 222 | | | | | |

[a] CC = cyclopentadienyl C atom; CR = $C_5$-ring centroid; C(*t*Bu) = *tert*-butyl C atom; Pl(1) = cyclopentadienyl mean plane.

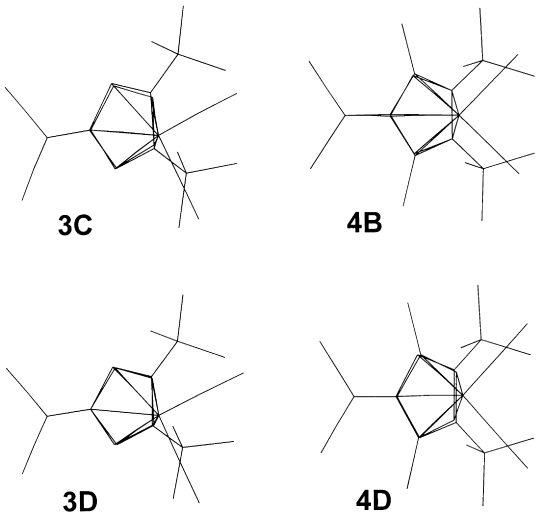


Fig. 4. Structures obtained with the $\eta^5$-model for the distorted dibromide and diiodide complexes **3C** and **3D** (left) and for the axially symmetric dichloride and diiodide complexes **4B** and **4D** (right), projected (with H atoms omitted) on the $ZrX_2$ plane.

parameters for these compounds, as well as those for the related, $C_2$-symmetric difluoride complex rac-$Me_2Si$(2-Me-4-$^t$Bu–$C_5H_2)_2ZrF_2$ (**4A**) are available from the Cambridge Crystallographic Data Center (e-mail: deposit@ccdc.cam.ac.uk) under quotation of deposit number CCDC 113624-113628, the authors and the journal reference of this article.

## Acknowledgements

Helpful discussions with Prof Brice Bosnich, University of Chicago, and with Prof Peter Comba, Universität Heidelberg, are gratefully acknowledged. We thank Dr Axel Rau, Perkin–Elmer Bodensee-Werk Überlingen, for help with the use of the Perkin–Elmer 2000 shuttle system and Dr Eberhard Heuser-Hofmann, Universität Konstanz, for help with the installation of the BIOSYMM program package. Financial support for this work was provided by BASF AG, Bundesminister für Forschung und

Table 8
Crystallographic structure determination data for compounds **3C**, **3D**, **4C** and **4D** (Conditions: Siemens P4 (**3C**, **3D**, **4D**) or Enraf Nonius CAD 4 (**4C**) four-circle diffractometer, Mo Kα radiation, graphite monochromator, $\omega$-scan mode. Solution with direct methods (SHELXS-86, G. M. Sheldrick, 1990). Anisotropic refinment for all non-hydrogen atoms. Hydrogen atoms refined on calculated positions with fixed isotropic $U$, using riding model techniques (SHELXL-93: G.M. Sheldrick, 1993). Absorption corrections with Ψ-scan data (Siemens XPREP-program))

| | **3C** | **3D** | **4C** | **4D** |
|---|---|---|---|---|
| Formula | $C_{20}H_{30}Br_2SiZr$ | $C_{20}H_{30}I_2SiZr$ | $C_{22}H_{34}Br_2SiZr\cdot(C_5H_{12})_{0.25}$ [a] | $C_{22}H_{34}I_2SiZr$ |
| Crystal color and form | Green prism | Orange needle | Green prism | Orange prism |
| Crystal size (mm) | 0.2 × 0.2 × 0.3 | 0.2 × 0.2 × 0.3 | 0.1 × 0.2 × 0.2 | 0.1 × 0.15 × 0.2 |
| Crystal system | Orthorhombic | Orthorombic | Monoclinic | Monoclinic |
| Space group | $Pca2_1$ | $Pca2_1$ | $P2_1/c$ | $P2_1/c$ |
| $a$ (Å) | 12.700(2) | 12.825(4) | 17.503(4) | 10.241(3) |
| $b$ (Å) | 10.404(2) | 10.778(2) | 15.651(2) | 14.613(5) |
| $c$ (Å) | 33.663(4) | 33.716(5) | 19.276(4) | 17.227(5) |
| $\beta$ (deg) | – | – | 99.490(10) | 93.31(3) |
| $V$ (Å$^3$), $Z$ | 4448.0(12), 8 | 4660.4(18), 8 | 5208.2(17), 8 | 2573.7(14), 4 |
| $d_{calc.}$ (g/cm$^3$) | 1.641 | 1.834 | 1.512 | 1.733 |
| $\mu$ (mm$^{-1}$), $F$(000) | 4.142, 2192 | 3.174, 2480 | 3.543, 2380 | 2.877, 1304 |
| $T$ (K) | 243 | 225 | 213 | 243 |
| $\theta$ range (°) | 2.30 to 27.00 | 2.24–30.5 | 1.69–22.99 | 2.37–27.99 |
| Reflections collected | 9776 | 14435 | 7498 | 6549 |
| Independent reflections | 9581 ($R_{int}$ = 0.0303) | 14209 ($R_{int}$ = 0.0276) | 7225 ($R_{int}$ = 0.0316) | 6216 ($R_{int}$ = 0.0285) |
| Observed reflections ($I > 2\sigma(I)$) | 7250 | 12503 | 4523 | 5009 |
| Number of parameters | 433 | 433 | 482 | 235 |
| GoF | 1.032 | 1.043 | 1.018 | 1.093 |
| $R(F)$, $R_W(F^2)$ | 0.0446, 0.0839 | 0.0336, 0.0782 | 0.0428, 0.0914 | 0.0374, 0.0843 |
| Weighting scheme: $a$, $b$ [b] | 0.0353, 3.887 | 0.0339, 5.832 | 0.043, 20.36 | 0.037, 4.412 |
| Largest diff. peak (e/Å$^3$) | 0.452 | 0.551 | 0.737 | 1.348 |

[a] The disordered pentane was refined isotropic. Hydrogen atoms of this molecule were neglected.
[b] $w^1 = \sigma^2(F_0^2) + (a\cdot P)^2 + b\cdot P$, with $P = (F_0^2 + 2F_c^2)/3$.

Technologie, Fonds der Chemischen Industrie and funds of the University of Konstanz.

## References

[1] H.H. Brintzinger, L.S. Bartell, J. Am. Chem. Soc. 92 (1970) 1105.
[2] H.H. Brintzinger, D. Fischer, R. Mühlhaupt, B. Rieger, R. Waymouth, Angew. Chemie Int. Ed. Engl. 34 (1995) 1143.
[3] V. Venditto, G. Guerra, P. Corradini, R. Fusco, Polymer 31 (1990) 531.
[4] L.A. Castonguay, A.K. Rappe, J. Am. Chem. Soc. 114 (1992) 2359.
[5] T.N. Doman, T.K. Hollis, B. Bosnich, J. Am. Chem. Soc. 117 (1995) 1352.
[6] B. Bosnich, Chem. Soc. Rev. 23 (1994) 387.
[7] U. Höweler, R. Mohr, M. Knickmeier, G. Erker, Organometallics 13 (1994) 2380.
[8] K. Angermund, A. Hanuschik, M. Nolte, in: G. Fink, R. Mülhaupt, H.H. Brintzinger (Eds.), Ziegler Catalysts, Springer, Berlin, 1995, pp. 251.
[9] Y. van der Leek, K. Angermund, M. Reffke, R. Kleinschmidt, R. Goretzki, G. Fink, Chem. Eur. J. 3 (1997) 585.
[10] Y.L. Slovokhotov, T.V. Timofeeva, Y.T. Struchkov, Zhur. Strukt. Khim. (Engl. Transl.) 28 (1987) 463.
[11] A.R. Kudinov, D.V. Muratov, M.I. Rybinskaya, P.V. Petrovskii, A.V. Mironov, T.V. Timofeeva, Y.L. Slovokhotov, Y.T. Struchkov, J. Organomet. Chem. 414 (1991) 97.
[12] K.E. Du Plooy, C.F. Marais, L. Carlton, R. Hunter, J.C.A. Boeyens, N.J. Coville, Inorg. Chem. 28 (1989) 3855.
[13] S.C. Mackie, M.C. Baird, Organometallics 11 (1992) 3712.
[14] J. Polowin, S.C. Mackie, M.C. Baird, Organometallics 11 (1992) 3724.
[15] P. Burger, J. Diebold, S. Gutmann, H.-U. Hund, H.H. Brintzinger, Organometallics 11 (1992) 1319.
[16] T.N. Doman, C.R. Landis, B. Bosnich, J. Am. Chem. Soc. 114 (1992) 7264.
[17] T.K. Hollis, J.K. Burdett, B. Bosnich, Organometallics 12 (1993) 3385.
[18] T.V. Timofeeva, J.-H. Lii, N.L. Allinger, J. Am. Chem. Soc. 117 (1995) 7452.
[19] P. Comba, Coord. Chem. Rev. 123 (1993) 1.
[20] P. Comba, T.W. Hambley, Molecular Modeling of Inorganic Compounds, VCH Weinheim, New York, 1995.
[21] P. Comba, M. Zimmer, J. Chem. Education 73 (1996) 108.
[22] B.P. Hay, Coord. Chem. Rev. 126 (1993) 177.
[23] B.P. Hay, Inorg. Chem. 30 (1991) 2876.
[24] P.V. Bernhardt, P. Comba, Inorg. Chem. 31 (1992) 2638.
[25] MOMEC97, a molecular modeling package for inorganic compounds, Lauer & Okon Chemische Verfahrens- & Softwareentwicklung, 1997.
[26] PCMODEL for WINDOWS 6.00, Serena Software, Bloomington, IN 47402-3076.
[27] Insight II Ver. 2.3.5, Discover 2.9.8: Molecular Simulations Inc., San Diego, CA 92121-3752.
[28] H.P. Fritz, Adv. Orgmet. Chem. I (1964) 239.
[29] E. Maslowsky Jr., Vibrational Spektra of Organometallic Compounds, Wiley, New York, 1977.
[30] P.M. Druce, B.M. Kingston, M.F. Lappert, T.R. Spalding, C. Srivastava, J. Chem. Soc. A (1969) 2106.
[31] E. Samuel, R. Ferner, M. Bigorgne, Inorg. Chem. 12 (1973) 881.
[32] E. Maslowsky Jr, K. Nakamoto, Appl. Spectrosc. 25 (1971) 187.
[33] P.M. Druce, B.M. Kingston, M.F. Lappert, R.C. Srivastava, M.J. Frazer, W.E. Newton, J. Chem. Soc. A (1969) 2814.
[34] M.-H. Prosenc, unpublished results.
[35] L.E. Schock, T.J. Marks, J. Am. Chem. Soc. 110 (1988) 7701.
[36] M.F. Ryan, J.R. Eyler, D.E. Richardson, J. Am. Chem. Soc. 114 (1992) 8611.
[37] M.A. Bush, G.A. Sim, J. Chem. Soc. A (1971) 2225.
[38] K. Prout, T.S. Cameron, R.A. Forder, S.R. Critchley, B. Denton, G.V. Rees, Acta Crystallogr. B30 (1974) 2290.
[39] M. Bühl, G. Hopp, W. von Philipsborn, S. Beck, M.-H. Prosenc, U. Rief, H.H. Brintzinger, Organometallics 15 (1996) 778.
[40] A. Antinolo, M.F. Lappert, A. Singh, D.J.W. Winterborn, L.M. Engelhardt, C.L. Raston, N.J. Taylor, J. Chem. Soc. Dalton Trans. (1987) 1463.
[41] C.S. Bajgur, W.R. Tikkanen, J.L. Petersen, Inorg. Chem. 24 (1985) 2539.
[42] H. Wiesenfeldt, A. Reinmuth, E. Barsties, K. Evertz, H.H. Brintzinger, J. Organomet. Chem. 369 (1989) 359.
[43] X. Yang, C.L. Stern, T.J. Marks, J. Am. Chem. Soc. 113 (1991) 3623.
[44] X. Yang, C.L. Stern, T.J. Marks, J. Am. Chem. Soc. 116 (1994) 10015.
[45] B. Heyn, B. Hipler, G. Kreisel, H. Schreer, D. Walther, Anorg. Synthesechemie, Springer, Berlin, 1986, p. 84.
[46] N. Klouras, H. Köpf, Monatsh. Chem. 112 (1981) 887.
[47] H. Köpf, N. Klouras, Z. Naturforsch 38B (1983) 321.
[48] Perkin–Elmer System 2000 Manual, pp. 2–56.